Supplementary Material (ESI) for Chemical Communications

Supporting Information for

Binuclear Cu(II) Coordination Complex Involving *Cis*-Tetrathiafulvalene-*Bis*-amido-2-pyridine-N-oxide as Bi-anionic Ligand: a Robust Molecular Precursor Toward Magnetic Conducting Materials

Fabrice Pointillart,[a] Thomas Cauchy,[b] Yann Le Gal,[a] Stéphane Golhen,[a] Olivier Cador[a] and Lahcène Ouahab*[a]

[a] Organométalliques et Matériaux Moléculaires, UMR 6226 CNRS-UR1 Sciences Chimiques de Rennes, Université de Rennes 1, 35042, Rennes Cedex, France. Fax : +33(0)2 23 23 68 40 ; Tel : +33(0)2 23 23 56 59 ; *lahcène.ouahab@univ-rennes1.fr*

[b] Chimie Théorique Inorganique, UMR 6226 CNRS-UR1 Sciences Chimiques de Rennes, Université de Rennes 1, 35042 Rennes Cedex, France.

Structural and Physical measurements. Single crystals were mounted on a Nonius four circle diffractometer equipped with a CCD camera and a graphite monochromated MoK_α radiation source (λ = 0.71073 Å), from the Centre de Diffractométrie (CDFIX), UR 1, France. Structure was solved with SIR-97 and refined with the SHELXL-97 program by full-matrix least-squares methods on F^2.[1] A SQUEEZE procedure was realised. Data are listed for all voids in the P1 unit cell, i.e. centre of gravity, solvent accessible volume, recovered number of electrons in the void (corresponding to a CH_2Cl_2 molecule) and details about the squeezed material is written in the cif file. Complete crystal structure results as a CIF file including bond lengths, angles, and atomic coordinates are deposited as Supporting Information. Cyclic voltametry was carried out in acetonitrile solution, containing 0.1 M $N(C_4H_9)_4PF_6$ as supporting electrolyte. Voltamograms were recorded at 100 $mV.s^{-1}$ at a platinum disk electrode. The potentials were measured *versus* a saturated calomel electrode (SCE). Optical spectra were measured using the KBr disk method on Perkin-Elmer 1600 Series FT-IR (resolution 4 cm^{-1}) for infrared (IR). Absorption spectra were recorded using the KBr disk method on a Varian Cary 5000 UV-Visible-NIR spectrometer equipped with an integration sphere.

Computational details. The UV-visible absorption spectra of the ligand *Cis/Trans*-**L** and complex **1** have been calculated. At first, a full geometry optimization of *Cis*-**L** has been carried out using Density Functional Theory (DFT) methods from the solid state geometry. All calculations were performed with the hybrid functional adaptation of PBE[2] (usually referred as PBE0) as implemented on the Gaussian03 program.[3] To manage calculation on the whole complex **1**, we used a double-ζ quality basis set proposed by Weigend et al. with polarization functions for all atoms.[4] Then, the first mono-electronic excitations (80 firsts) were computed using a Time Dependant Density Functional Theory (TD-DFT) procedure with the same program, functional and basis set as the first step.

1 (a) Otwinowski, Z.; Minor, W. Processing of X-ray Diffraction Data Collected in Oscillation Mode. *In Methods in Enzymology, Volume 276: Macromolecular Crystallography, Part A*. (b) Carter, C. W.; Sweet, R. M. Jr. Eds.; Academic Press: 1997; pp 307-326. (c) G. M. Sheldrick, SHELXL-97, Program for refinement of crystal structures, University of Göttingen, Germany, 1997.

2 Perdew, J. P.; Burke, K.; Ernzerhof, M. *Phys. Rev. Lett.*, **1996**, 77, 3865; (b) Adamo, C.; Barone, V. *J. Chem. Phys.*, **1999**, *110*, 6158.

3 Frisch, M. J.; Trucks, G. W.; Schlegel, H. B.; Scuseria, G. E.; Robb, M. A.; Cheeseman, J. R.; Montgomery, J. A.; Vreven, T.; Kudin, K. N.; Burant, J. C.; Millam, J. M.; Iyengar, S. S.; Tomasi, J.; Barone, V.; Mennucci, B.; Cossi, M.; Scalmani, G.; Rega, N.; Petersson, G. A.; Nakatsuji, H.; Hada, M.; Ehara, M.; Toyota, K.; Fukuda, R.; Hasegawa, J.; Ishida, H.; Nakajima, T.; Honda, Y.; Kitao, O.; Nakai, H.; Klene, M.; Li, X.; Knox, J. E.; Hratchian, H. P.; Cross, J. B.; Adamo, C.; Jaramillo, J.; Gomperts, R.; Stratmann, R. E.; Yazyev, O.; Austin, A. J.; Cammi, R.; Pomelli, C.; Ochterski, J.; Ayala, P. Y.; Morokuma, K.; Voth, G. A.; Salvador, P.; Dannenberg, J. J.; Zakrzewski, V. G.; Dapprich, S.; Daniels, A. D.; Strain, M. C.; Farkas, O.; Malick, O. K.; Rabuck, A. D.; Raghavachari, K.; Foresman, J. B.; Ortiz, J. V.; Cui, Q.; Baboul, A. G.; Clifford, S.; Cioslowski, J.; Stefanov, B. B.; Liu, G.; Liashenko, A.; Piskorz, P.; Komaromi, I.; Martin, R. L.; Fox, D. J.; Keith, T.; Al-Laham, M. A.; Peng, C. Y.; Nanayakkara, A.; Challacombe, M.; Gill, P. M. W.; Johnson, B.; Chen, W.; Wong, M. W.; Gonzalez, C.; Pople, J. A. Gaussian 03 (Revision D.02) ed., Gaussian, Inc, Pittsburgh, PA, **2003**.

4 Weigend, F.; Ahlrichs, R. *Phys. Chem. Chem. Phys.*, **2005**, *7*, 3297.

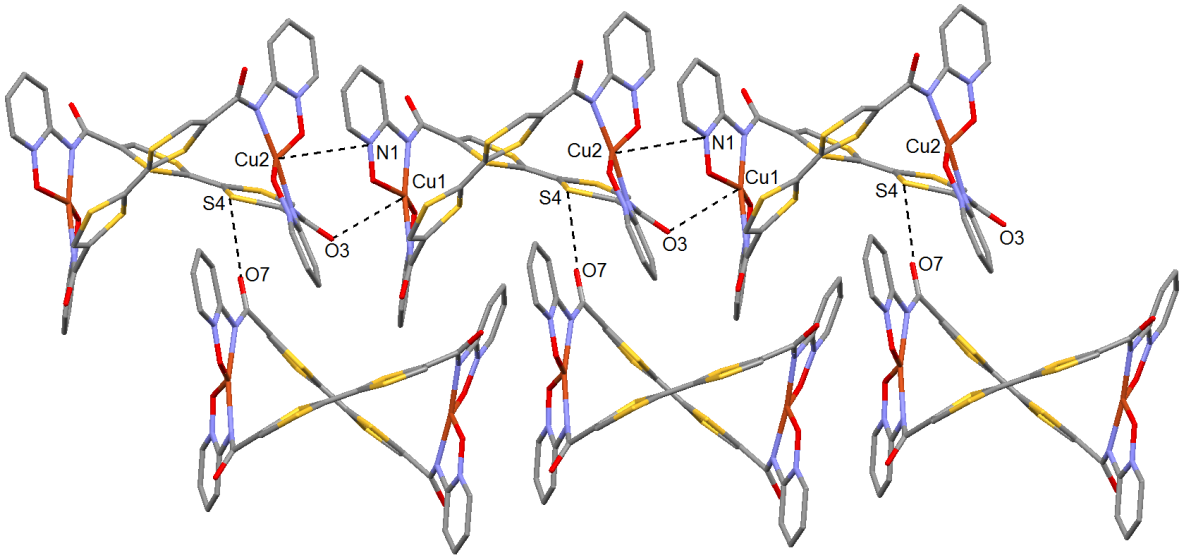

Fig. S1 Packing view of the dinuclear complex {Cu_2[*Cis*-TTF-*Bis*-CON-2-Py-N-oxide)]$_2$} (**1**) along the b axis highlighting the short contacts.

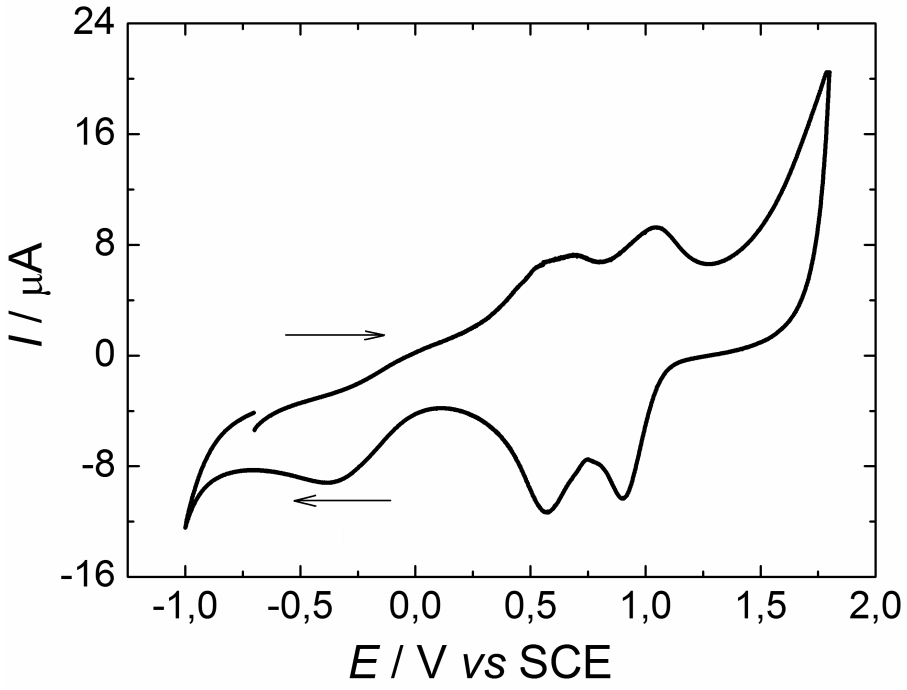

Fig. S2 Cyclic voltammetry of the ligand *Cis/Trans*-**L** in CH_2Cl_2 at a scan rate of 100 mV.s^{-1}.The potentials were measured *versus* a saturated calomel electrode (SCE); glassy carbon as the working electrode; Pt wire as the counter electrodes.

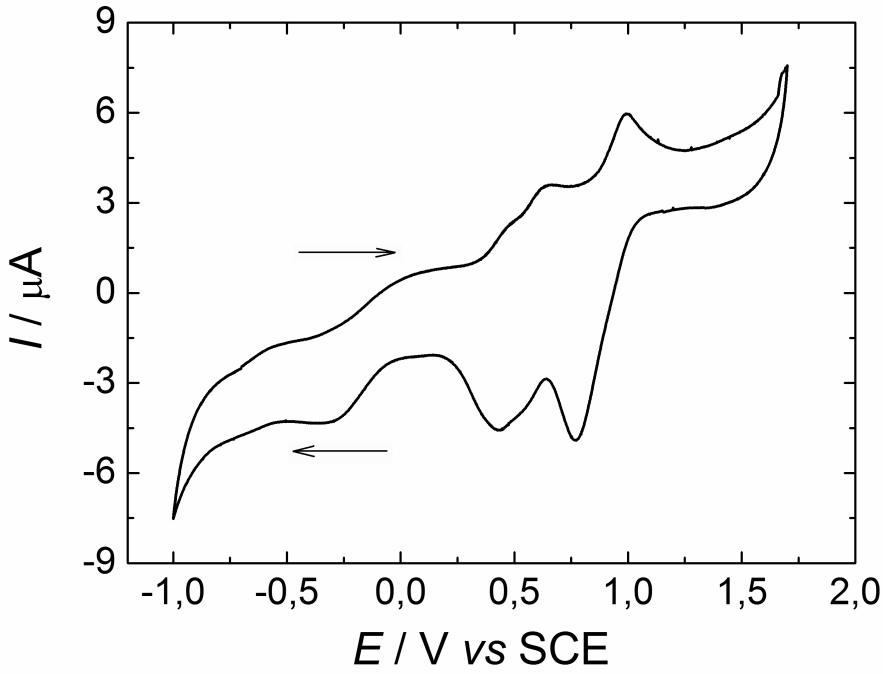

Fig. S3 Cyclic voltammetry of the complex **1** in CH_2Cl_2 at a scan rate of 100 mV.s^{-1}.The potentials were measured *versus* a saturated calomel electrode (SCE); glassy carbon as the working electrode; Pt wire as the counter electrodes.

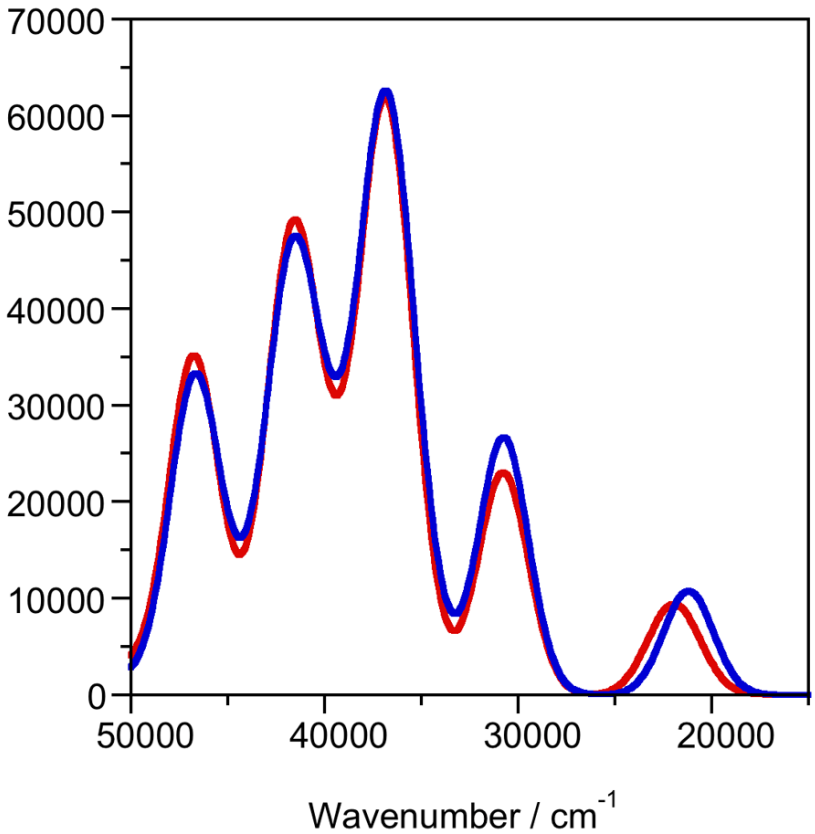

Fig. S4 Red and blue lines represent respectively the theoretical absorption spectra of *Cis*-**L** in C_{2v} symmetry and the *Trans*-**L** in C_1 symmetry structures.

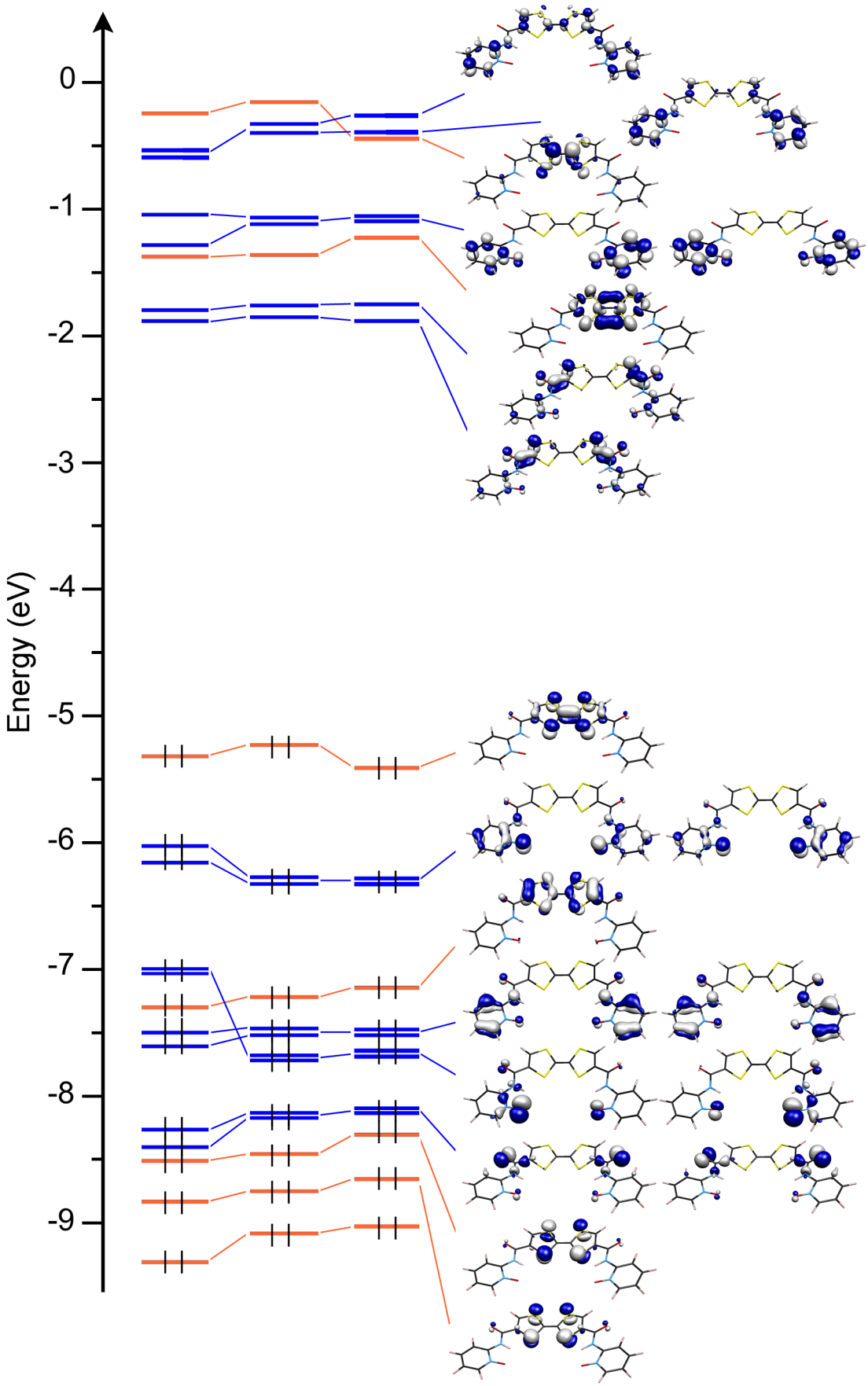

Fig. S5 Molecular orbital diagram of the solid-state structure (left), a C_{2v} symmetry (middle) and a C_1 symmetry structure (right) of *Cis*-**L**.

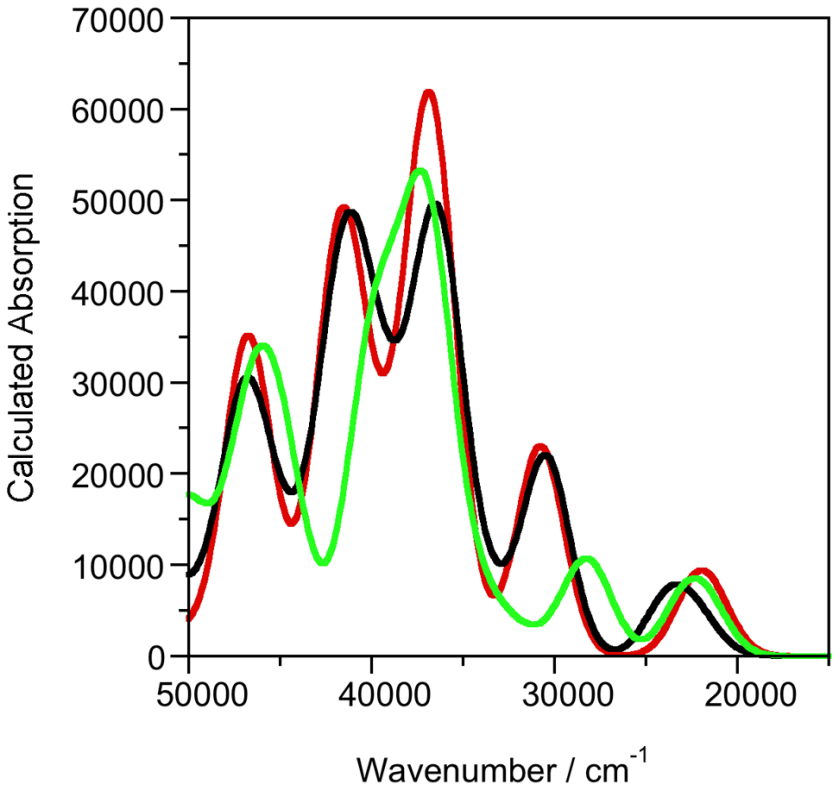

Fig. S6 Red, black and green lines represent respectively the theoretical absorption spectra of *Cis*-**L** in C_{2v} symmetry, C_1 symmetry and the solid-state structures.

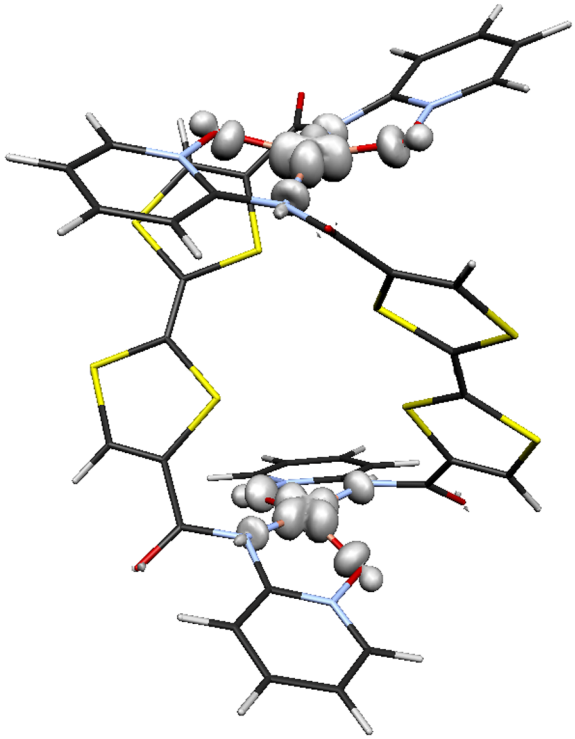

Fig. S7 Spin density distribution of the solid-state structure of **1**, corresponding to the most stable S = 1.* The isodensity surface represented corresponds to a value of 0.005 e^-/bohr^3 (positive values are represented as white surfaces and no negative values are observed).

* The magnetic susceptibility measurements show that there is no significant intramolecular magnetic interaction between the two copper cations in the molecule. Therefore, both singlet and triplet state have almost the same energy. Calculations on the singlet state are not straightforward as it is a polydeterminantal state (a mixture of the up-down and down-up determinants), in contrary the triplet state is correctly described by the monodeterminantal approach employed (DFT).

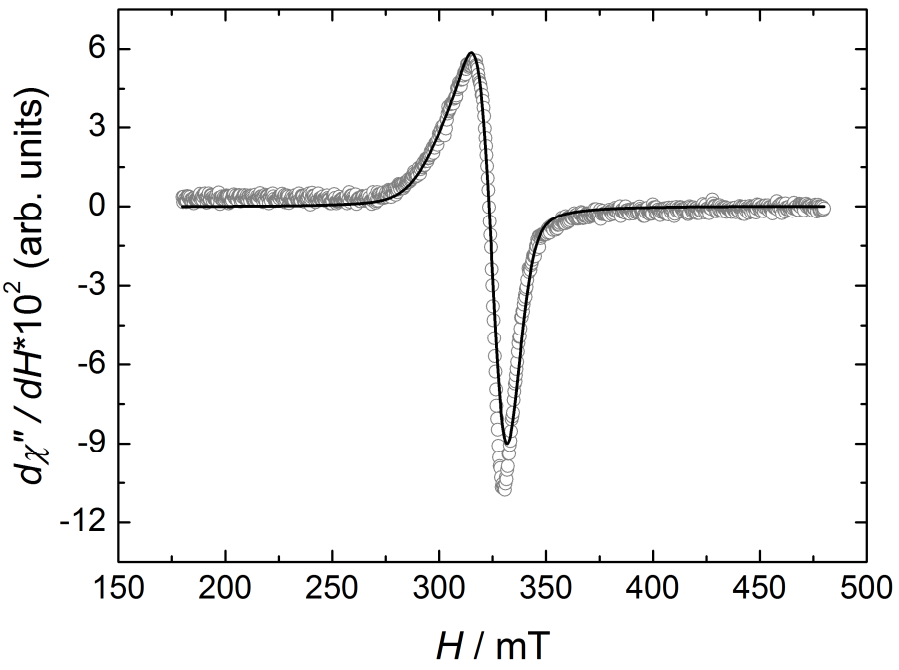

Fig. S8 Experimental X-Band (9.470 GHz) EPR spectrum of crunched single crystals of **1** at 67 K (gray circles) and its best simulation (full black line).

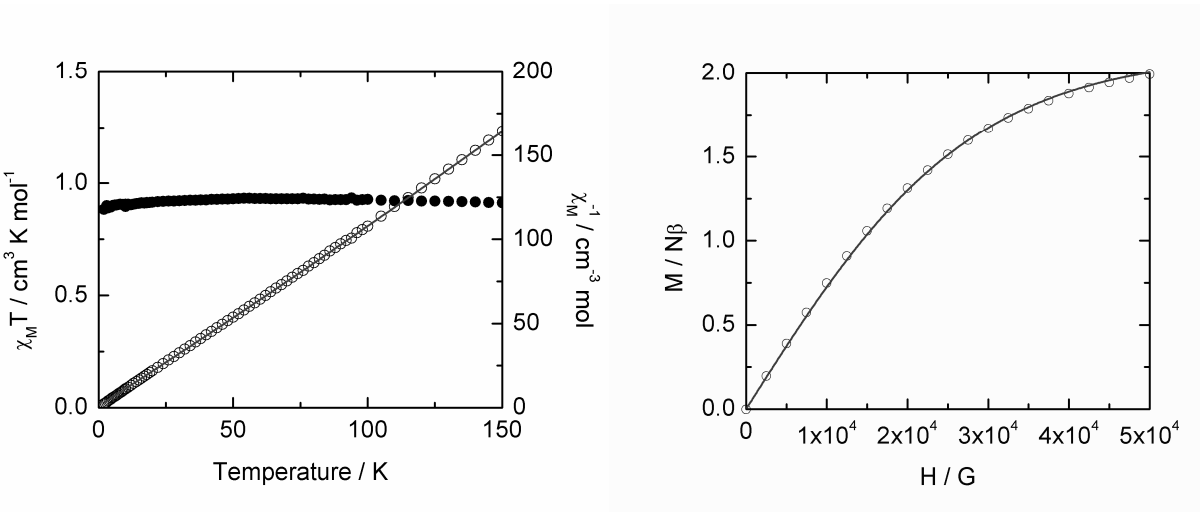

Fig. S9 (On the left) $1/\chi_M$ *vs* T (open circles) with fits to the Curie-Weiss law (black solid line) and $\chi_M T$ *vs* T (closed circles) for **1**. (On the right) Experimental field dependence of the magnetization for **1** (open circles) and calculated magnetization for uncorrelated spin system (black solid line).

Table S1. TD-DFT calculated energies of the low-lying electronic excitations associated with an oscillator factor $f \geq 0.05$, of solid-state structure of *Cis*-**L**.

Energy (cm^{-1})	λ (nm)	Osc.	Transition
21790	459	0.06	Ho→Lu (77%), Ho→Lu+2 (10%), Ho→Lu+1 (5%)
22880	437	0.07	Ho→Lu+1 (66%), Ho→Lu+2 (26%)
27855	359	0.07	Ho-1→Lu (51%), Ho-1→Lu+1 (36%)
36805	272	0.35	Ho→Lu+7 (30%), Ho-5→Lu+3 (23%), Ho-1→Lu+5 (6%), Ho-8→Lu+1 (6%)
37189	269	0.18	Ho-8→Lu (26%), Ho→Lu+7 (21%), Ho-8→Lu+1 (17%), Ho-5→Lu+1 (8%)
37736	265	0.08	Ho-5→Lu (13%), Ho-5→Lu+1 (13%), Ho-9→Lu+1 (11%), Ho→Lu+7 (11%), Ho→Lu+9 (10%), Ho-9→Lu (10%), Ho-1→Lu+5 (7%)
38730	258	0.08	Ho-1→Lu+5 (19%), Ho-1→Lu+4 (14%), Ho-3→Lu+1 (14%), Ho-9→Lu+1 (9%), Ho-9→Lu (6%)
39200	255	0.06	Ho-2→Lu+6 (21%), Ho-5→Lu (19%), Ho-8→Lu+1 (8%), Ho-5→Lu+1 (6%), Ho-8→Lu (5%)
39968	250	0.14	Ho-6→Lu (24%), Ho-3→Lu+2 (16%), Ho-5→Lu+1 (13%), Ho-6→Lu+1 (12%), Ho-1→Lu+4 (8%)
40193	249	0.07	Ho-5→Lu+1 (28%), Ho-6→Lu (17%), Ho-6→Lu+1 (14%), Ho-3→Lu+2 (6%)
40552	246	0.07	Ho-7→Lu (40%), Ho-7→Lu+1 (20%), Ho-5→Lu+1 (10%)
44385	225	0.06	Ho-6→Lu+2 (75%), Ho-5→Lu+3 (8%)
45065	222	0.12	Ho-7→Lu+3 (32%), Ho-7→Lu+2 (28%), Ho-2→Lu+8 (16%)
46147	217	0.07	Ho-2→Lu+8 (47%), Ho-5→Lu+4 (10%), Ho-7→Lu+3 (10%), Ho-10→Lu+2 (6%)
46620	215	0.07	Ho-1→Lu+9 (48%), Ho-6→Lu+4 (20%), Ho-10→Lu (11%)
47015	213	0.06	Ho→Lu+11 (35%), Ho-10→Lu (28%), Ho-6→Lu+4 (8%), Ho-10→Lu+1 (7%)
50454	198	0.16	Ho-6→Lu+5 (59%), Ho-6→Lu+6 (7%), Ho-11→Lu (5%)

Table S2. TD-DFT calculated energies of the low-lying electronic excitations associated with an oscillator factor $f \geq 0.05$, of C_1 symmetry structure of *Cis*-**L**.

Energy (cm^{-1})	λ (nm)	Osc.	Transition
22075	453	0.04	Ho→Lu (87%)
23753	421	0.08	Ho→Lu+1 (93%)
30211	331	0.09	Ho-1→Lu (57%), Ho-2→Lu+1 (21%), Ho→Lu+4 (8%)
30488	328	0.12	Ho-2→Lu (38%), Ho→Lu+3 (36%), Ho-1→Lu+1 (15%)
30769	325	0.09	Ho→Lu+3 (61%), Ho-2→Lu (23%), Ho-1→Lu+1 (7%)
35587	281	0.16	Ho-3→Lu (18%), Ho→Lu+5 (12%), Ho-1→Lu+3 (11%), Ho-4→Lu+1 (10%), Ho-2→Lu+4 (10%), Ho-5→Lu (8%)
36232	276	0.13	Ho-1→Lu+4 (17%), Ho-2→Lu+3 (14%), Ho-4→Lu (13%), Ho-5→Lu+1 (9%), Ho-2→Lu+6 (7%), Ho-2→Lu+2 (6%)
36765	272	0.34	Ho→Lu+5 (20%), Ho→Lu+7 (17%), Ho→Lu+9 (14%)
38911	257	0.10	Ho-3→Lu+1 (55%), Ho-1→Lu+4 (16%), Ho-2→Lu+3 (12%)
39370	254	0.12	Ho-3→Lu+2 (68%), Ho→Lu+9 (11%), Ho→Lu+5 (5%)
40816	245	0.10	Ho-5→Lu (42%), Ho-1→Lu+6 (16%), Ho-2→Lu+7 (8%), Ho-4→Lu+1 (8%), Ho-2→Lu+5 (7%)
40984	244	0.20	Ho-4→Lu (42%), Ho-2→Lu+6 (18%), Ho-1→Lu+7 (9%), Ho-5→Lu+1 (8%), Ho-1→Lu+5 (8%)
41667	240	0.13	Ho-6→Lu+4 (15%), Ho-7→Lu (10%), Ho-1→Lu+6 (10%), Ho-7→Lu+3 (9%), Ho-5→Lu (8%), Ho-2→Lu+4 (7%), Ho-1→Lu+3 (5%), Ho-6→Lu (5%)
41841	239	0.13	Ho-7→Lu+3 (13%), Ho-7→Lu (12%), Ho-6→Lu+4 (12%), Ho-1→Lu+6 (10%), Ho-5→Lu (8%), Ho-2→Lu+4 (7%), Ho-1→Lu+3 (6%)
42918	233	0.08	Ho-4→Lu+1 (57%), Ho-5→Lu (16%), Ho-2→Lu+5 (14%)
45249	221	0.07	Ho-10→Lu (43%), Ho-5→Lu+2 (36%), Ho-10→Lu+2 (6%)
46860	213	0.07	Ho-6→Lu+2 (46%), Ho-4→Lu+3 (11%), Ho-5→Lu+4 (11%), Ho-10→Lu+1 (7%)
46926	213	0.13	Ho-6→Lu+2 (27%), Ho-2→Lu+8 (17%), Ho-4→Lu+3 (11%), Ho-5→Lu+4 (10%), Ho-1→Lu+9 (9%), Ho-1→Lu+7 (6%), Ho-7→Lu+2 (6%)
47170	212	0.09	Ho-1→Lu+9 (38%), Ho-2→Lu+8 (26%), Ho-4→Lu+3 (8%), Ho-5→Lu+4 (8%)
51282	195	0.07	Ho→Lu+13 (64%), Ho-3→Lu+8 (8%), Ho→Lu+11 (7%)

Table S3. TD-DFT calculated energies and assignments of the low-lying electronic excitations associated with an oscillator factor $f \geq 0.05$, of C_{2v} symmetry structure of *Cis*-**L**. D, A, Ho, Lu and *nb* represent respectively the TTF (Donor), the *pyNO* (Acceptor), the HOMO, the LUMO and a non-bonding orbital, therefore DACT stands for Donor to Acceptor Charge Transfer and ID for Intra-Donor.

Exp Energy (cm^{-1})	Calcd Energy (cm^{-1})	Osc.	Type	Assignment	Transition
21920	**21446**	**0.05**	**DACT**	$\pi^{nb}_{D}\rightarrow\pi^{*}_{A}$	**Ho→Lu (92%)**
	22263	**0.08**	**DACT**	$\pi^{nb}_{D}\rightarrow\pi^{*}_{A}$	**Ho→Lu+1 (92%)**
32180	30609	0.10	IA	$\pi^{nb}_{A}\rightarrow\pi^{*}_{A}$	Ho-1→Lu (54%), Ho-2→Lu+1 (28%), Ho-2→Lu+4 (4%), Ho-1→Lu+3 (4%)
	30896	**0.21**	**IA**	$\pi^{nb}_{A}\rightarrow\pi^{*}_{A}$	**Ho-2→Lu (52%), Ho-1→Lu+1 (29%), Ho-2→Lu+4 (4%), Ho-1→Lu+3 (4%)**
41390	35824	0.14	IA	$\pi^{nb}_{A}\rightarrow\pi^{*}_{A}$	Ho-1→Lu+3 (14%), Ho-2→Lu+4 (14%), Ho→Lu+7 (13%), Ho-4→Lu+1 (13%), Ho-5→Lu (11%), Ho-3→Lu (9%), Ho-1→Lu+5 (4%), Ho-2→Lu+6 (4%), Ho-5→Lu+3 (2%), Ho-2→Lu+1 (2%)
	36229	0.14	IA	$\pi^{nb}_{A}\rightarrow\pi^{*}_{A}$	Ho-1→Lu+4 (19%), Ho-2→Lu+3 (17%), Ho-4→Lu (14%), Ho-5→Lu+1 (11%), Ho-2→Lu+5 (7%), Ho-1→Lu+6 (6%), Ho-1→Lu+1 (5%), Ho-2→Lu (3%), Ho-3→Lu+1 (3%), Ho-4→Lu+3 (3%), Ho-5→Lu+4 (2%)
	37127	**0.62**	**ID**	$\pi^{nb}_{D}\rightarrow\pi^{*}_{D}$	**Ho→Lu+7 (48%), Ho→Lu+6 (6%), Ho-2→Lu+4 (5%), Ho-1→Lu+3 (4%), Ho-3→Lu (4%), Ho-2→Lu+1 (3%), Ho-1→Lu+5 (3%), Ho-2→Lu+6 (2%)**
	39348	0.12	DACT	$\pi^{nb}_{D}\rightarrow\pi^{*}_{A}$	Ho-3→Lu+1 (80%), Ho-2→Lu+3 (5%), Ho-1→Lu+4 (3%)
	41166	0.11	IA	$\pi^{nb}_{A}\rightarrow\pi^{*}_{A}$	Ho-5→Lu (35%), Ho-1→Lu+5 (17%), Ho-2→Lu+6 (15%), Ho-4→Lu+1 (12%), Ho-4→Lu+4 (4%), Ho-5→Lu+3 (3%)
	41247	**0.18**	**IA**	$\pi^{nb}_{A}\rightarrow\pi^{*}_{A}$	**Ho-4→Lu (34%), Ho-2→Lu+5 (19%), Ho-1→Lu+6 (17%), Ho-5→Lu+1 (12%), Ho-5→Lu+4 (4%), Ho-4→Lu+3 (4%)**
	41979	**0.34**	**IA**	$\pi^{nb}_{A}\rightarrow\pi^{*}_{A}$	**Ho-1→Lu+5 (18%), Ho-5→Lu (15%), Ho-2→Lu+4 (14%), Ho-2→Lu+6 (13%), Ho-1→Lu+3 (12%), Ho-4→Lu+1 (2%)**
48390	**46646**	**0.15**	**IA**	$\pi^{nb}_{A}\rightarrow\pi^{*}_{A}$	**Ho-10→Lu (44%), Ho-5→Lu+3 (16%), Ho-4→Lu+4 (16%), Ho-11→Lu+1 (5%), Ho-7→Lu+2 (3%), Ho-2→Lu+7 (2%)**
	46932	**0.30**	**IA**	$\pi^{nb}_{A}\rightarrow\pi^{*}_{A}$	**Ho-4→Lu+3 (32%), Ho-5→Lu+4 (30%), Ho-10→Lu+1 (5%), Ho-1→Lu+6 (4%), Ho-2→Lu+5 (3%), Ho-1→Lu+7 (3%), Ho-6→Lu+2 (2%), Ho-11→Lu (2%)**

Table S4. TD-DFT calculated energies and assignment of the most pertinent low-lying electronic excitations, associated with an oscillator factor $f \geq 0.01$ of **1**. D, A, Ho, Lu and *nb* represent respectively the TTF (Donor), the *pyNO* (Acceptor), the HOMO, the LUMO and a non-bonding orbital, therefore DACT stands for Donor to Acceptor Charge Transfer.

Energy (cm^{-1})	λ (nm)	Osc.	Type	Assignment	Transition
20881	479	0.01	DACT	$\pi^{nb}_{D}\rightarrow\pi^{*}_{A}$	Ho-1β→Lu+2β (30%), Ho-1α →Luα (27%), Ho-1β→Lu+10β (10%), Ho-1α→Lu+8α (9%), Ho-1β→Lu+8β (6%), Ho-1α→Lu+6α (5%)
21277	470	0.03	DACT	$\pi^{nb}_{D}\rightarrow\pi^{*}_{A}$	Hoα→Lu+1α (36%), Hoβ→Lu+3β (33%), Hoβ→Lu+7β (7%), Hoβ→Lu+5β (7%)
21538	464	0.01	DACT	$\pi^{nb}_{D}\rightarrow\pi^{*}_{A}$	Ho-1β→Lu+10β (13%), Ho-1α →Lu+1α (12%), Ho-1α →Luα (11%), Ho-1α→Lu+8α (9%), Ho-1β→Lu+4β (9%), Ho-1β→Lu+2β (9%), Ho-1β→Lu+6β (8%)
21915	456	0.01	DACT	$\pi^{nb}_{D}\rightarrow\pi^{*}_{A}$	Hoβ→Lu+4β (28%), Ho-1β→Lu+3β (19%), Hoβ→Lu+5β (15%), Hoα→Lu+3α (12%), Ho-1α→Lu+1α (5%)
22007	454454	0.03	DACT	$\pi^{nb}_{D}\rightarrow\pi^{*}_{A}$	Hoβ→Lu+4β (25%), Hoβ→Lu+5β (11%), Hoα→Lu+3α (10%), Ho-1α→Lu+2α (10%), Ho-1β→Lu+4β (7%), Hoα→Lu+2α (5%)
23026	434	0.02	DACT	$\pi^{nb}_{D}\rightarrow\pi^{*}_{A}$	Hoα→Lu+5α (36%), Hoβ→Lu+6β (23%), Hoβ→Lu+7β (16%), Hoβ→Lu+3β (11%), Hoα→Lu+1α (7%)
24085	415	0.01	DACT	$\pi^{nb}_{D}\rightarrow\pi^{*}_{A}$	Ho-1β→Lu+7β (34%), Ho-1β→Lu+8β (23%), Hoα→Lu+6α (18%)
24248	412	0.01	DACT	$\pi^{nb}_{D}\rightarrow\pi^{*}_{A}$	Ho-1β→Lu+7β (34%), Hoα→Lu+6α (16%), Ho-1β→Lu+8β (11%), Ho-1β→Lu+9β (8%), Ho-1β→Lu+6β (7%)

Table S5. Theoretical composition of frontier orbitals of solid-state structure of **1**.

MO	eV	%Cu	%D	%A	Assignment	MO	eV	%Cu	%D	%A	Assignment	equiv TTFNO
Lu+9	-0.62	0	74	25	σ^*_D	Lu+11	-0.62	0	75	25	σ^*_D	Lu+2
Lu+8	-0.75	3	77	20	σ^*_D	Lu+10	-0.72	3	76	20	σ^*_D	Lu+2
Lu+7	-1.01	0	12	87	π^*_A	Lu+9	-0.98	2	14	84	π^*_A	Lu+1/Lu
Lu+6	-1.05	0	24	76	π^*_A	Lu+8	-1.05	0	23	76	π^*_A	Lu+1/Lu
Lu+5	-1.16	1	24	76	π^*_A	Lu+7	-1.11	5	21	74	π^*_A	Lu+1/Lu
Lu+4	-1.18	0	14	85	π^*_A	Lu+6	-1.16	0	21	79	π^*_A	Lu+1/Lu
Lu+3	-1.29	1	20	80	π^*_A	Lu+5	-1.23	4	16	80	π^*_A	Lu+1/Lu
Lu+2	-1.34	0	9	90	π^*_A	Lu+4	-1.31	2	7	92	π^*_A	Lu+1/Lu
Lu+1	-1.40	1	11	88	π^*_A	Lu+3	-1.37	1	5	94	π^*_A	Lu+1/Lu
Lu	-1.47	1	6	93	π^*_A	Lu+2	-1.46	1	5	94	π^*_A	Lu+1/Lu
						Lu+1	-2.11	60	4	36	d*	
						Lu	-2.20	58	5	37	d*	
Ho	-4.61	0	83	17	π^{nb}_D	Ho	-4.61	0	83	17	π^{nb}_D	Ho
Ho-1	-4.65	1	83	16	π^{nb}_D	Ho-1	-4.64	1	83	16	π^{nb}_D	Ho
Ho-2	-6.24	5	5	91	π^{nb}_A	Ho-2	-6.16	6	4	90	π^{nb}_A	Ho-1
Ho-3	-6.32	5	4	91	π^{nb}_A	Ho-3	-6.22	7	3	90	π^{nb}_A	Ho-1
Ho-4	-6.46	5	45	50	π^{nb}_L	Ho-4	-6.55	1	69	30	π^{nb}_D	Ho-2
Ho-5	-6.56	1	72	27	π^{nb}_D	Ho-5	-6.55	0	77	22	π^{nb}_D	Ho-2
Ho-6	-6.61	9	8	84	π^{nb}_A	Ho-6	-6.69	4	13	83	π^{nb}_A	Ho-1
Ho-7	-6.71	4	34	63	π^{nb}_L	Ho-7	-6.72	4	7	89	π^{nb}_A	Ho-1
Ho-8	-6.91	12	6	82	$\pi^{nb}_A/p^{nb}_{O(CO)}$	Ho-8	-7.21	6	6	89	π^{nb}_A	Ho-3
Ho-9	-6.95	13	12	74	$\pi^{nb}_A/p^{nb}_{O(CO)}$	Ho-9	-7.26	7	2	91	π^{nb}_A	Ho-3
Ho-10	-7.30	3	5	92	π^{nb}_A	Ho-10	-7.28	2	11	86	π^{nb}_A	Ho-3
Ho-11	-7.35	3	8	90	$\pi^{nb}_A/p^{nb}_{O(CO)}$	Ho-11	-7.30	5	7	88	$p^{nb}_{O(CO)}$	Ho-4
Ho-12	-7.36	3	7	91	$\pi^{nb}_A/p^{nb}_{O(CO)}$	Ho-12	-7.33	4	10	86	$\pi^{nb}_A/p^{nb}_{O(CO)}$	Ho-3/-4
Ho-13	-7.39	2	9	89	π^{nb}_A							
Ho-14	-7.43	2	6	92	π^{nb}_A							
Ho-15	-7.49	2	17	82	$p^{nb}_{O(CO)}$	Ho-13	-7.40	2	17	81	$p^{nb}_{O(CO)}$	Ho-4
Ho-16	-7.63	7	13	81	$p^{nb}_{O(CO)}$	Ho-14	-7.44	2	11	86	$p^{nb}_{O(CO)}$	Ho-4
Ho-17	-7.73	7	12	81	$p^{nb}_{O(CO)}$	Ho-15	-7.54	3	13	84	$p^{nb}_{O(CO)}$	Ho-4
Ho-18	-7.76	2	65	33	π^{nb}_D	Ho-16	-7.73	3	63	34	π^{nb}_D	Ho-5
Ho-19	-7.89	1	57	41	π^{nb}_D	Ho-17	-7.87	1	58	41	π^{nb}_D	Ho-5